

pubs.acs.org/JPCC Article

# Stacking of Monolayer Graphene Particles at a Water-Vapor Interface

David M. Goggin,<sup>#</sup> Ronghua Bei,<sup>#</sup> Ryther Anderson, Diego A. Gómez-Gualdrón, and Joseph R. Samaniuk<sup>\*</sup>



Cite This: J. Phys. Chem. C 2021, 125, 7880-7888



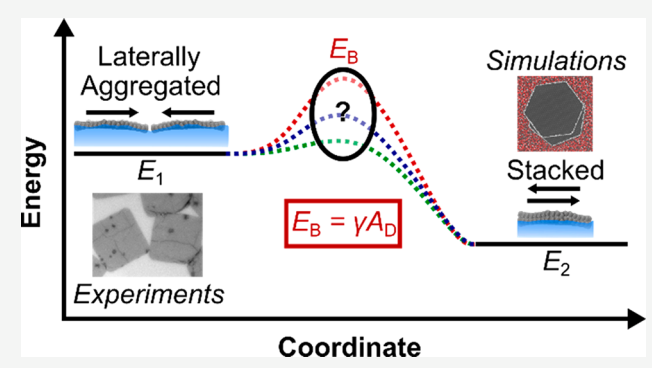
**ACCESS** 

III Metrics & More

Article Recommendations

SI Supporting Information

ABSTRACT: Two-dimensional (2D) materials such as graphene prefer to interact in a face-to-face manner when colloidally suspended but are forced to interact in an edge-to-edge manner when trapped at a fluid—fluid interface. However, molecular dynamics (MD) simulations suggest these platelet-like particles can spontaneously stack and adopt the preferred face-to-face orientation after lateral edge-to-edge assembly, while experiments tend to contradict these findings. Thus, conditions under which these stacking events occur are unknown. Herein, MD simulations are employed to elucidate the physical origin of the free-energy barrier inhibiting instantaneous particle stacking: the surface energy penalty associated with deforming a fluid—fluid interface. Simulations suggest stacking kinetics are governed by a Boltzmann-like



relation between the time to stack and the particle—particle contact edge length, and thus, the interfacial area deformed. A thermodynamic model is also shown to predict the change in excess interfacial free-energy as particles transition from the laterally aggregated to vertically stacked state at a fluid interface. Finally, experimental evidence is presented that corroborates these results. These results suggest that the existence of nanometer-scale edge defects is expected to influence the stacking behavior of 2D particles at fluid interfaces, which has broad, practical implications spanning from emulsion stability to the integrity of Langmuir film morphology.

# **■ INTRODUCTION**

Liquid-phase exfoliated two-dimensional (2D) materials, such as graphene, are a class of platelet-like particles that have colloidal-scale lateral dimensions but atomic-scale thicknesses. The molecularly thick nature of 2D materials leads to thickness-dependent properties such that a desired property can be tuned by varying the number of stacked layers, up to the bulk phase property limit.<sup>2</sup> Fluid-fluid interfaces can therefore be exploited to confine and laterally assemble 2D materials into thin films with uniform thickness, which is critical to achieving the desired properties in thin-film applications such as optoelectronics<sup>3,4</sup> and photoelectrochemical catalysis.<sup>5</sup> Additionally, 2D materials have found uses as "particle surfactants" because of their ability to irreversibly adsorb, stabilize, and impart functionality (e.g., thermal/electrical conductivity, photoacoustic properties, etc.) to the fluid-fluid interfaces ubiquitous in emulsions and foams.<sup>6,7</sup> Thus, it is imperative to understand the (thermo)dynamics of 2D materials at fluidfluid interfaces given the breadth of disciplines in which these systems find applications.

A dynamic unique to 2D materials at fluid interfaces is particle stacking. Molecular dynamics (MD) simulations indicate that laterally aggregated, monolayer graphene particles

can stack on top of one another without the assistance of mechanical compression, 4,8 wherein one of the particles is able to detach from the fluid–fluid interface and "slide" over the neighboring particle. This spontaneous stacking dynamic present between 2D materials has never been observed for spherical colloidal (spheroidal) particles at fluid interfaces, which have been observed to detach, buckle, or form bilayer films at fluid interfaces upon overcompression of the film, 9,10 and can be reasoned by examining the length scales involved in the two systems.

The schematic in Figure 1a shows top-down and side views of a spheroidal particle and hexagonal monolayer graphene particle. In the plane of a fluid–fluid interface (top view), the spheroidal and graphene particles have comparable characteristic length scales,  $L_{\rm c}$ . This explains why 2D materials are irreversibly pinned to fluid interfaces like spheroidal

Received: December 24, 2020 Revised: March 11, 2021 Published: April 7, 2021





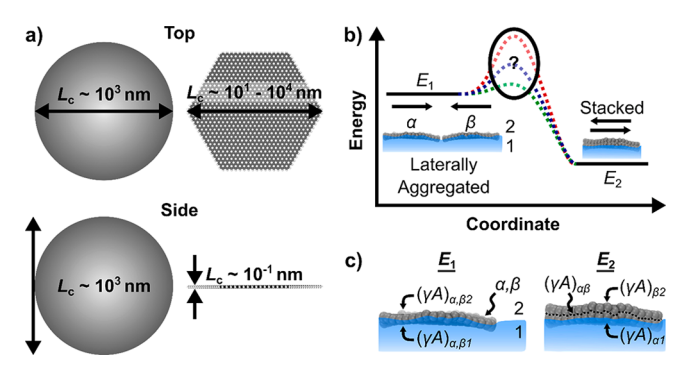


**Figure 1.** (a) Schematic of top view and side view of a spheroidal particle (left) and monolayer graphene particle (right) demonstrating the difference in characteristic length scales  $L_{\rm c}$  in-plane with (top) and normal to (side) a fluid—fluid interface. (b) Schematic representation of the free-energy diagram that laterally aggregated monolayer graphene particles in energy state  $E_1$  must follow to stack and find the minimum energy state of the system  $E_2$ . (c) Schematic showing the excess interfacial free-energy associated with various interfaces used in the calculation of eq 1.

particles. 11,12 However, the characteristic length scales of a spheroidal and monolayer graphene particle are vastly different in the direction normal to the plane of the interface (side view). Spheroidal particles are isotropic and maintain a characteristic length scale ( $\sim 10^3$  nm) that is much greater than the thickness of a fluid-fluid interface ( $\sim 10^{-1}-10^{0}$ nm),13,14 while monolayer graphene particles have a thickness  $(\sim 10^{-1} \text{ nm})$  that is commensurate with the length scales of out-of-plane thermal motions of a fluid-fluid interface (i.e., capillary waves).<sup>15</sup> This results in graphene particles being more sensitive to thermal fluctuations of a fluid-fluid interface<sup>16</sup> than spheroidal particles, and small variations in the position of graphene particles normal to the interface could induce neighboring graphene particles to overlap and stack due to attractive, face-to-face van der Waals forces, <sup>17</sup> as observed in MD simulations.<sup>4,8</sup> Yet, there is an apparent discord between simulations and experiments, as experimental evidence has demonstrated laterally aggregated and only partially overlapped monolayer particles even after compression to high particle densities. 11,18,19

A thermodynamic argument, shown schematically in Figure 1b,c further highlights the discrepancies observed between experiments and simulations. By calculating the excess interfacial free-energy associated with the initial laterally aggregated state,  $E_1$ , and the final stacked particle configuration,  $E_2$ , the change in excess interfacial free-energy,  $\Delta E$ , associated with stacking two graphene particles can be given by (derivation in Supporting Information)

$$\Delta E = (\gamma_{12} + \gamma_{\alpha\beta} - \gamma_{\alpha2} - \gamma_{\beta1})A \tag{1}$$

where  $\gamma_{12}$  is the fluid—fluid interfacial tension,  $\gamma_{\alpha\beta}$  is the surface energy between two graphene particles,  $\gamma_{\alpha2}$  is the surface energy between particle  $\alpha$  and the upper fluid,  $\gamma_{\beta1}$  is the surface energy between particle  $\beta$  and the lower fluid, and A is the contact area between two entities, for example, graphene-upper fluid phase, graphene-lower fluid phase, etc. (Figure 1c). We have assumed the two interacting graphene particles are the same size. Using  $\gamma_{12}\approx 50$  mJ m $^{-2}$  (oil—water interface),  $\gamma_{\alpha2}\approx 40$  mJ m $^{-2}$  (graphene-oil),  $\gamma_{\beta1}\approx 80$  mJ m $^{-2}$  (graphene-water),  $\gamma_{\alpha2}\approx 0$  mJ m $^{-2}$  (graphene-graphene), and  $\gamma_{\beta1}\approx 0$ 0 mJ m $^{-2}$ 0 (graphene-graphene), and  $\gamma_{\beta1}\approx 0$ 1 m $\gamma_{\beta1}\approx 0$ 2 mJ m $\gamma_{\beta2}\approx 0$ 3 mJ m $\gamma_{\beta1}\approx 0$ 3 mJ m $\gamma_{\beta2}\approx 0$ 4 mJ m $\gamma_{\beta2}\approx 0$ 5 mJ m $\gamma_{\beta2}\approx 0$ 7 mJ m $\gamma_{\beta2}\approx 0$ 7 mJ m $\gamma_{\beta3}\approx 0$ 8 mJ m $\gamma_{\beta4}\approx 0$ 9 mJ m $\gamma_{\beta4}\approx$ 

order of magnitude of  $\Delta E$  is obtained for graphene at an airwater interface. We have assumed  $\gamma_{\alpha\beta} \approx 0$  mJ m<sup>-2</sup> because this value is used for approximate calculations, and two graphene monolayers should have a negligibly small excess interfacial free-energy between them (see Supporting Information). Additionally, we have neglected the influence of line tension on the excess interfacial free-energy of the system as we are interested in solving this problem to a first approximation, and because of the variation in the reported magnitude, sign, and effect of line tension on the detachment of nanoparticles from fluid interfaces.<sup>20</sup> Furthermore, we show in the Results and Discussion section that our results align with what is predicted in eq 1 ( $\Delta E$ ) and eq 3 ( $E_B$ ), which suggests that our primary approximations to solve for the thermodynamics and dynamics of graphene particle stacking capture the most significant physics present in this system; however, investigating line tension effects would be valuable in future efforts. This large negative change in excess interfacial free-energy suggests that the stacking of monolayer graphene particles should be highly favorable at fluid-fluid interfaces, and that stacking is most likely an irreversible process. However, we know stacking is not instantaneous because it is possible to experimentally observe films containing unstacked monolayer particles in apparent lateral contact after deposition from a fluid interface, and stacking is not observed during direct observation of the particles at fluid-fluid interfaces. <sup>21</sup> This analysis implies there must be a significant energy barrier preventing instantaneous particle stacking.

In this work, we use MD simulations to understand the dynamics and thermodynamics of monolayer graphene particle-monolayer graphene particle stacking at a watervapor interface. We use nonbiased simulations to analyze the time required for laterally aggregated particles to stack as a function of the contact edge length between particles and the interfacial area deformed. We find a single exponential function can describe each relation. Additionally, we use the adaptive biasing force (ABF) algorithm<sup>22-24</sup> to extract potential of mean force (PMF) diagrams and elucidate the physical origin of the energy barrier preventing particle stacking. Biased simulations indicate the energy barrier to particle stacking is related to the surface energy penalty associated with deforming a fluid-fluid interface by a given interfacial area, which increases as the contact edge length between particles increases. Furthermore, biased simulations demonstrate that our thermodynamic model proposed in eq 1 can predict the excess interfacial free-energy change of the system associated with two graphene particles transitioning from the laterally aggregated to the vertically stacked state. Finally, we present experimental images of laterally aggregated, monolayer graphene particles at an air-water interface that help explain why the stacking of monolayer graphene particles at fluid-fluid interfaces is not likely to be observed on experimental time scales. This work addresses discrepancies previously observed between simulations and experiments and provides a detailed analysis of fundamental dynamics and thermodynamics of monolayer graphene particles at fluid-fluid interfaces. The key findings of (i) the contact edge length between adjacent particles governing stacking dynamics and (ii) the development of an empirical model to predict the conditions under which particle stacking may occur are expected to have tremendous impact on the design and implementation of exfoliated 2D materials for use at fluid-fluid interfaces depending on the desired end application.

#### METHODS

**Simulation Details.** The initial configurations of graphene particles in the simulations were generated using PACK-MOL.<sup>25</sup> Simulations were performed with graphene particles modeled as hexagons (Figure 2b) and rectangles (Figure 2c).

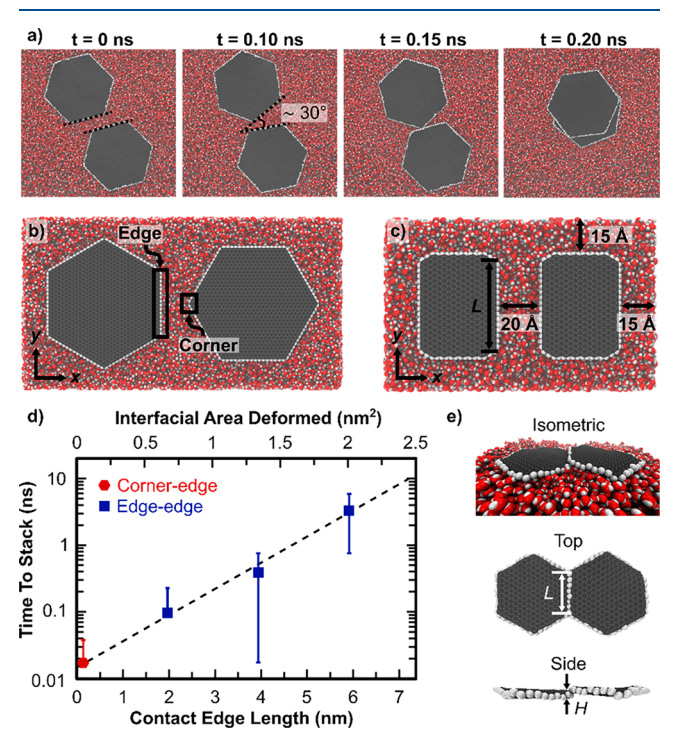


Figure 2. (a) Time lapse of two hexagonal graphene particles that were allowed free translation and rotation. Immediate stacking occurred when particles adopted a corner-to-edge configuration and were in lateral contact. Small hexagonal particles had an in-plane diffusion coefficient of 1.3 nm<sup>2</sup> ns<sup>-1</sup> and large hexagonal particles had an in-plane diffusion coefficient of 0.32 nm<sup>2</sup> ns<sup>-1</sup>. (b) Initial configuration of graphene particles simulated as hexagons and (c) as rectangles in simulations that forced particles to only interact in the x-direction (y-momentum and angular momentum were fixed) with a desired contact edge length L. (d) Time required to stack as a function of the contact edge length (lower x-axis) and the corresponding interfacial area deformed,  $A_{\rm D}$  = LH (upper x-axis), where L and H are defined in panel e. The red hexagon represents the average value acquired from corner-to-edge simulations, and blue squares represent the average values obtained from edge-to-edge simulations. Error bars represent one standard deviation from the average. The black dashed line is an exponential fit for the time to stack as a function of the interfacial area deformed data. (e) Three different views of two particles at the moment stacking was initiated. The interfacial area deformed is determined by the contact length L between two interacting particles and the thickness H of a graphene monolayer.

Particles were separated by 20 Å from edge-to-edge and 15 Å from the edge of each particle to the boundaries of the simulation cell (Figure 2c). The graphene particles were initially fixed while the energy of the water molecules was minimized. The graphene particles were then released and allowed to fluctuate and explore the surface at constant volume and constant temperature, 298 K (NVT conditions). The equations of motion were integrated with a time step  $t_{\rm s}=1$  fs in all cases. A Nosé-Hoover thermostat was used with the temperature damping parameter set to  $100t_{\rm s}$ . The length of time that simulations were allowed to run before termination

depended on the timing of the expected event. For example, in simulations where stacking was concerned, the simulations were terminated shortly after stacking was observed. For the simulations where graphene particles were only allowed to translate in the x-direction, the y-momentum and angular momentum of each graphene structure were set to zero. This forced the graphene particles to interact with a predetermined lateral configuration when the particles arrived at close contact. Molecular dynamics simulations reported in this study were performed using LAMMPS (large-scale atomic/molecular massively parallel simulator), <sup>26</sup> version 7 Aug 2019, an opensource molecular dynamics program from Sandia National Laboratories. Simulation trajectories were visualized using VMD (version 1.9.3) with a time step between output frames of 0.001 ns  $(1000t_s)$  for the edge-to-corner (Figure 2b) simulations and 0.05 ns  $(50000t_s)$  for all other simulations.

Models for Pure Components. The various graphene structures were modeled with the AIREBO force field. 27 All three terms of the AIREBO force field (REBO, Lennard-Jones (LJ), and torsion) were turned on, with the cutoff of longranged interactions set to 8.5 Å. The graphene particles were terminated with edge hydrogen atoms. Water molecules were modeled using the SPC/E force field with a LJ interaction cutoff of 9 Å and long-range electrostatic interactions.<sup>28</sup> The PPPM long-range electrostatic solver was used with an accuracy of  $10^{-4}$ . The surface tension of the water-vapor interface was calculated to be  $56.1 \pm 21.2$  mN m<sup>-1</sup> using the thermodynamic method without the tail correction introduced by Ismail et al.<sup>29</sup> In agreement with previous studies,<sup>30,31</sup> the simulated surface tension of the water-vapor interface modeled with the SPC/E force field was shown to underestimate the experimental surface tension of water (~72 mN m<sup>-1</sup>) at room temperature because of the truncation of the LJ and electrostatic interactions.<sup>21</sup>

We note the surface tension and error reported in our work  $(56.1 \pm 21.2 \text{ mN/m})$  were calculated by averaging the surface tension calculated at each time step in a single simulation after the energy of the water molecules had been minimized, and the reported error (±21.2 mN/m) represents one standard deviation from this temporal average. To investigate why the reported error was so large, we performed 10 independent simulations and again measured the surface tension for each simulation using the thermodynamic method in Ismail et al. 2006.<sup>29</sup> The average (arithmetic mean) surface tension was calculated to be 54.5  $\pm$  0.7 mN/m for the N = 10 replicates, which is again in agreement with the average and deviation in surface tension reported by Ismail et al. for a water-vapor interface at  $\sim$ 300 K simulated using the SPC/E model (55.4  $\pm$ 2.4 mN/m).<sup>29</sup> However, closer inspection of the temporal deviation within each of the 10 independent simulations showed that each simulation had a temporal deviation of  $\sim$ 23 mN/m, which agreed with our initially presented results of  $56.1 \pm 21.2$  mN/m. Given that the value we are seeking to quantify is a fundamentally transient phenomenon (i.e., the time to stack after particles have made lateral contact), use of the large error reported for the temporal average of the surface tension is more appropriate than that obtained from an arithmetic mean across a given number of simulations because at any given time step in the simulation the instantaneous surface tension can swing from  $\sim$ 35 mN/m up to  $\sim$ 75 mN/m, which will either decrease or increase the energy barrier required for particles to stack given that the energy barrier is also dependent on the surface tension of the system (eq 3).

This also helps explain why we also observe large error bars associated with the data in Figure 2d and Figure 3c.

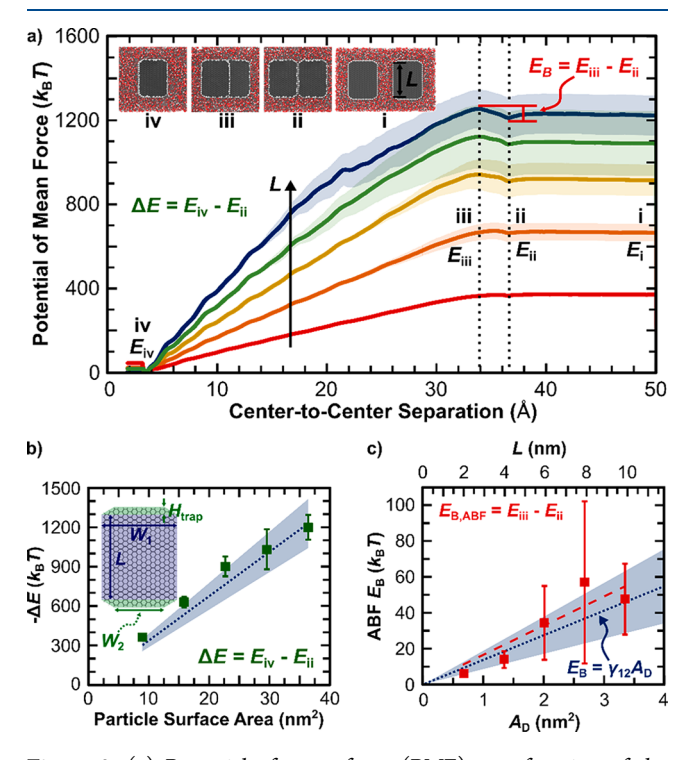


Figure 3. (a) Potential of mean force (PMF) as a function of the center-to-center separation of two interacting graphene particles. The contact edge length L between the two interacting particles increases from the bottom to top curves. Inset images in upper left depict the relative configuration of particles at various energy states  $E_i$  (j = i, ii, etc.) in the PMF curve: (i) initial separation, (ii) lateral aggregation, (iii) initial overlap, (iv) completely stacked. The free-energy barrier  $E_{\rm B}$ that particles must overcome to stack is depicted in the upper right. The change in excess interfacial free-energy of the system  $\Delta E$  from the laterally aggregated state is depicted in the middle left. (b) Change in excess interfacial free-energy  $\Delta E$  as a function of the particle surface area. The inset image shows the particle surface area, which is calculated only on one side of the particle. Green squares represent the average values obtained from PMF plots and the dashed blue line represents the values predicted by eq 1. Error bars represent one standard deviation from the average values obtained from PMF plots, and the shaded blue region represents one standard deviation from the average  $-\Delta E$  values predicted using eq 1 and the error in the simulated water-vapor surface tension  $\gamma_{12} = 56.1 \pm 21.2 \text{ mN m}^{-1}$ . (c) Energy barriers (red squares) calculated from PMF plots as a function of the interfacial area deformed (lower x-axis) and contact edge length (upper x-axis). Error bars represent one standard deviation from the average. The dashed red line is a linear fit to the data with respect to the interfacial area deformed. The blue dotted line represents the average energy barrier predicted by eq 3. The shaded blue region is estimated error from the barrier predicted by eq 3 and was calculated from the standard deviation in the simulated water-vapor surface tension  $\gamma_{12} = 56.1 \pm 21.2 \text{ mN m}^{-1}$ .

**Model for the Water–Graphene Interactions.** Water and graphene particles interacted through Lennard-Jones pair potentials with parameters  $\varepsilon_{\rm CO}$  (kJ mol<sup>-1</sup>) = 0.392,  $\sigma_{\rm CO}$  (Å) = 3.19,  $\varepsilon_{\rm CH}$  (kJ mol<sup>-1</sup>) = 0, and  $\sigma_{\rm CH}$  (Å) = 0.<sup>32</sup> These interactions were truncated at 12.5 Å.<sup>32</sup>

**Potential of Mean Force Calculations.** The adaptive biasing force method in the LAMMPS collective variable (Colvars) module was used in the simulations for which

potential of mean force (PMF) plots were calculated.  $^{23,33}$  The ABF method output the PMF on the *y*-axis and the distance between the centers of the two graphene particles on the *x*-axis. The applied force was scaled using a factor between 0 and 1 before at least 200 samples had been collected in each distance bin to avoid nonequilibrium effects due to potential fluctuations of the force exerted during the process of two graphene particles coming into contact. Once at least 200 samples were collected the scaling factor was set to 1. The Jacobian term was excluded for the distance-based variable in this study.

Unbiased Simulations: Time to Stack After Contact. Initial simulations were performed that allowed two identical,

hexagonal graphene particles to freely rotate and translate

across a water-vapor interface. Two particle sizes were chosen

for these initial simulations, with particle parameters given in

#### RESULTS AND DISCUSSION

Supporting Information Table S1. These systems were referred to as "small" particle simulations and "large" particle simulations, respectively. Small hexagonal particles had edge lengths of 1.97 nm and single-sided surface areas of 10.1 nm<sup>2</sup>, and large hexagonal particles had edge lengths of 3.94 nm and surface areas of 40.3 nm<sup>2</sup>. The magnitudes of the particle sizes were not chosen to correspond to any specific experimental conditions, but rather the variation in size ratio was chosen, specifically the doubling of the edge lengths, because the size ratio can also be varied experimentally. The preliminary hypothesis was that the large particle simulations would require a longer time to stack once laterally aggregated than the smaller particle simulations because of the 2× increase in edge length and ~4× increase in particle surface area. The rationale for this hypothesis was that an increase in either edge length or particle area should require greater energy barriers to be overcome to displace a larger particle from a fluid-fluid interface. However, we observed that two large hexagonal particles would stack in approximately the same amount of time after they had laterally aggregated as two small hexagonal particles that had laterally aggregated. Further examination of the orientation of the small and large particles immediately before stacking demonstrated that rapid stacking would occur if the interacting particles rotated from the initial edge-to-edge alignment and adopted a corner-to-edge orientation upon lateral particle contact as shown in the sequential images in Figure 2a. To understand these results, we performed

simulations using the large particles described above, but

rotated one of the particles by 30° so the initial configuration

was set to a corner-to-edge orientation (Figure 2b). The

angular rotation of both hexagonal particles was fixed, and

particles were only allowed to translate in the x-direction. This

forced particles to interact with a specific contact edge length L

(shown in Figure 2c), which in the corner-to-edge config-

uration was a carbon–carbon double bond with  $L \approx 0.14$  nm

(i.e., the length of the corner). Over an average of 15 simulations, the time required for particles to stack once

laterally aggregated in the corner-to-edge configuration was

 $0.017 \pm 0.021$  ns (Figure 2d). The error reported is one

standard deviation from the average. These preliminary results

suggested the *contact* edge length of two interacting graphene particles determined the time required for particle stacking,

and not the *absolute* edge length nor the total particle area. Further simulations were performed between two identical, rectangular particles to test the new hypothesis that contact

edge length governed the time scale for particle stacking (Figure 2c). Particles again were not allowed to rotate around the z-axis nor translate in the y-direction. The rotational bias prevented the particles from rotating to a more favorable orientation for stacking (i.e., corner-edge vs edge-edge) before or after lateral aggregation, but the bias did not otherwise influence the energy barriers that would influence the time to stack. Rectangular particles were chosen instead of hexagonal particles because we were interested only in varying the contact edge length, and rectangular particles allowed for a smaller simulation cell and greater computational efficiency. Rectangular particles were also chosen for simulations to represent the experimental case of edge-to-edge aggregation of graphene particles, and hexagonal particles were chosen to represent the experimental case of corner-to-edge aggregation. The shape of the particles did not influence the simulation results (Figure S1). We observed an exponential relation between the time required for stacking to occur (after particles had first made lateral contact) and the contact edge length  $L_{i}$ and the interfacial area deformed,  $A_D = LH$ , (Figure 2d) where H is the thickness of a graphene monolayer (H = 0.34 nm,Figure 2e).<sup>34</sup> The thickness of the particles was held constant across all simulations. Note the calculated time to stack only accounted for the elapsed time between the first frame where two particles were observed in lateral contact and the first frame where particle overlap was observed, and not the total elapsed time from the start of the simulation. All results were analyzed with respect to the interfacial area deformed because of the physical origin of the energy penalty associated with deforming a planar fluid-fluid interface.

An increase in the surface area of a fluid—fluid interface is energetically unfavorable. Thus, an increase in the contact edge length L of two laterally aggregated graphene particles (Figure 2c,e) should result in an increase in the total water—vapor interfacial area that must be deformed in order for the two particles to stack. This interfacial deformation manifests as a surface energy penalty  $E_{\rm S}$  that scales linearly with  $A_{\rm D}$  as  $E_{\rm S} \propto \gamma_{12}A_{\rm D}$ , where  $\gamma_{12}$  is the water—vapor surface tension given in mN m<sup>-1</sup> or mJ m<sup>-2</sup>. Additionally, the Boltzmann distribution suggests that the probability  $p_i$  of finding a system in a given energy state relative to the probability  $p_j$  of finding the same system in a different energy state is described by the relation

$$\frac{p_i}{p_j} = \exp\left[\frac{-(E_i - E_j)}{k_{\rm B}T}\right] \tag{2}$$

where  $E_k$  is the energy of the system in state i or j.<sup>36</sup> If we assume  $E_i$  is the energy of the system when the two particles are in edge-to-edge contact (i.e., the reference energy state), and let  $E_i$  be the energy of the system when one of the particles deforms the interface (i.e., the surface energy penalty,  $E_i = E_s =$  $\gamma_{12}A_{\rm D}$ ), we find that larger differences between  $E_i$  and  $E_i$  result in a lower probability of finding the system in the higher energy state. This result is reasonable as it is less probable for the spontaneous deformation of a large area of water-vapor interface than for the spontaneous deformation of a small area of water-vapor interface. Thus, the exponential relationship observed between the time required for particles to stack and the interfacial area deformed (dashed black line, Figure 2d) agrees well with this simple Boltzmann distribution analysis. The exponential fit of the data  $(R^2 = 0.994)$  resulted in a relation of  $t_{\text{stack}} = 0.015 \exp(2.63A_{\text{D}})$ .

Biased Simulations: Potential of Mean Force Diagrams. The adaptive biasing force (ABF) algorithm<sup>22,23</sup> is a powerful computational tool that can extract the free-energy landscape of various physical systems studied using molecular dynamics simulations.<sup>24</sup> A key feature of the ABF method is its ability to flatten peaks and valleys in the free-energy profile of the system of interest and allow the system to explore energy states that are kinetically hindered in unbiased MD simulations.<sup>24</sup> This feature allowed us to perform ABF simulations of particles with larger edge lengths than in non-ABF (i.e., unbiased) MD simulations. Figure 3a presents the potential of mean force as a function of the center-to-center distance between two identical, rectangular graphene particles that were not allowed to rotate, nor translate in the y-direction. The parametric variable in Figure 3a is the contact edge length of the two interacting graphene particles. Two observations are immediately noticeable as the contact edge length L of the two graphene particles increases (moving from the bottom to the top curve): we observe a larger change in free-energy  $\Delta E$  from the laterally aggregated state  $(E_{ii})$  to the stacked state  $(E_{iv})$  as Lincreases, and we observe an increase in the size of the energy barrier,  $E_{\rm B}$ , with increasing L.

Figure 3b shows the change in excess interfacial free-energy associated with the transition from the laterally aggregated state to the vertically stacked state as a function of the graphene particle surface area. The change in excess interfacial free-energy was calculated as the energy difference between the local energy minimum at ~37 Å, when the particles are laterally aggregated, Eii in Figure 3a, and the global energy minimum at ~3.4 Å, when the particles are stacked in the preferred graphite interlayer spacing distance,  $E_{iv}$  in Figure 3a. The particle surface area was calculated by neglecting the thickness of graphene and by only calculating the area of one face of a pseudorectangular graphene particle, shown as the inset image in Figure 3b and enlarged in Figure S2. Each particle was assumed to have a surface area of  $A_{\rm part} = A_{\rm rect} + 2$ ·  $A_{\text{trap}}$  comprising a rectangular section of area  $A_{\text{rect}} = LW_1$ , where  $W_1$  is the width of the particle including the hydrogen (H)-terminated edges, and two trapezoidal sections of area  $A_{\text{trap}} = H_{\text{trap}} \cdot (W_1 + W_2)/2$ , where  $H_{\text{trap}}$  is the height of the trapezoidal area including the H-terminated edges and  $W_2$  is the width of the small segment parallel to  $W_1$ . The green squares are the values of  $\Delta E$  acquired from the ABF simulations, and error bars represent one standard deviation from the average, where the average was taken over at least N =15 simulations for each data point. The dashed blue line represents the theoretical  $\Delta E$  values calculated using eq 1 with values of  $\gamma_{12} = 56.1 \text{ mN m}^{-1}$  (simulated water-vapor interfacial tension, see the Methods section for details),  $\gamma_{a2}$  $\approx$  115 mJ m<sup>-2</sup> (graphene–water vapor),<sup>37</sup>  $\gamma_{\beta 1} \approx$  80 mJ m<sup>-2</sup> (graphene–water),<sup>8,37</sup> and  $\gamma_{\alpha\beta} \approx$  0 mJ m<sup>-2</sup> (graphene– graphene), and the contact area  $A = A_{part}$ . The blue shaded region represents error from the theoretical  $\Delta E$  values predicted by eq 1 and was calculated from the standard deviation in the simulated water-vapor surface tension  $\gamma_{12}$  =  $56.1 \pm 21.2$  mN m<sup>-1</sup>. We note the statistical error generally increases with increasing particle size, which we hypothesize is due to less efficient or incomplete sampling for larger systems.<sup>24</sup> This situation could be remedied by allowing the larger systems to run for a longer amount of time. However, the nice agreement between the  $\Delta E$  values obtained from ABF simulations and those from our proposed thermodynamic relation (eq 1) suggest the ABF simulations capture the most important excess interfacial free-energy changes corresponding to the system transitioning from the laterally aggregated to the vertically stacked energy state, and an increase in the time the larger systems are allowed to run should improve the accuracy while maintaining the same trends as above.

Figure 3c plots the average free-energy barrier calculated from the ABF simulations (red squares) as a function of the water-vapor interfacial area deformed for stacking to occur. All of the ABF simulations were performed using rectangular graphene particles, but the results are independent of particle shape. The energy barrier was calculated as the free-energy difference between the free-energy of the peak at ~34 Å (when the particles have just begun to overlap,  $E_{iii}$  in Figure 3a) and the free-energy of the valley at  $\sim$ 37 Å (when the particles are laterally aggregated,  $E_{ii}$  in Figure 3a). We observed the results could be fit  $(R^2 = 0.954)$  with a linear relation of  $E_{B,ABF} =$  $16.30A_D$ , shown as the dashed red line in Figure 3c. These results agree with our findings in Figure 2d; particles that must deform a larger interfacial area before stacking can occur must overcome a larger free-energy barrier and therefore require a longer time to stack. Thus, we argue the free-energy barrier  $E_{\rm B}$ that needs to be overcome for monolayer graphene particles to transition from a laterally aggregated to a vertically stacked state at a water-vapor interface is governed by the surface energy penalty  $E_S$  associated with deforming the interface, and is given by

$$E_{\rm B} = E_{\rm S} = \gamma_{12} A_{\rm D} \tag{3}$$

Notably, eq 3 should also apply to other fluid-fluid interfaces (e.g., oil-water) if the interfacial tension  $\gamma_{12}$  is known. The blue dotted line in Figure 3c plots eq 3 using the surface tension calculated from our system ( $\gamma_{12} = 56.1 \pm 21.2 \text{ mN}$ m<sup>-1</sup>). The blue shaded region surrounding the broken line represents one standard deviation from the average theoretical energy barrier due to the uncertainty in the calculated surface tension. The ABF-generated free-energy barriers are slightly larger than the values predicted by eq 3 at larger values of  $A_D$ . This could arise from the neglected contribution of the mechanical energy required to bend the graphene particle and not just deform the interface, 4,38 as well as the dependency of the Young's modulus on graphene particle size up to ~10 nm.<sup>39</sup> However, our results are informative as they represent a lower bound on the energy barrier preventing particle stacking (with the exception that line tension has been neglected), and any contribution from the mechanical bending energy would only increase the energy barrier to particle stacking.

Again, it is notable that the error bars on the ABF-generated data increase with increasing contact edge length, and thus overall particle size. As the ABF algorithm only adds a biasing force along the reaction coordinate, in this case the center-tocenter particle separation distance, there is no guarantee the transition state will look the same for every free-energy barrier crossing. Thus, the increased deviation in the ABF-generated free-energy barriers with increasing system size could arise from more transition states being observed. While increased sampling would reduce error and increase accuracy, the agreement between the ABF-generated and theoretically predicted free-energy barriers suggests that the main contribution to the free-energy barrier preventing laterally aggregated monolayer graphene particles from stacking on one another comes from the energy penalty required to deform the water-vapor interface, which is a key result from these biased simulations that was previously unknown.

We note that all simulations that experienced the initial particle overlap transition state always resulted in the completely stacked orientation and never remained fixed in the partially overlapped state. Sinclair et al. noted that force fields used to model graphene-graphene interactions using only Lennard-Jones nonbonded interactions, such as the AIREBO force field employed in our work, underestimate the friction between adjacent graphene layers<sup>40</sup> and could explain why we always observed complete overlap in our MD simulations. We expect the potential of mean force plots would have more local energy barriers preventing further particle translation after the two graphene particles had overlapped (e.g., center-to-center distances from  $\sim 34$  Å to  $\sim 3.4$  Å in Figure 3a) if the GraFF force field employed by Sinclair et al.<sup>40</sup> was used instead of the AIREBO force field. This would occur because of the additional friction that arises when attempting to displace stacked graphene particles from their preferred stacked orientation, which is accounted for in the GraFF force field. However, we do not expect the choice of force field used to model graphene-graphene interactions to affect our results as the  $\Delta E$  values presented are state functions, and the freeenergy barrier inhibiting particle stacking is dependent only on the interfacial tension, lateral contact length between particles, and particle thickness.

**Experimental Observations.** Figure 4 shows an assembly of 25  $\mu$ m monolayer graphene squares that had self-assembled

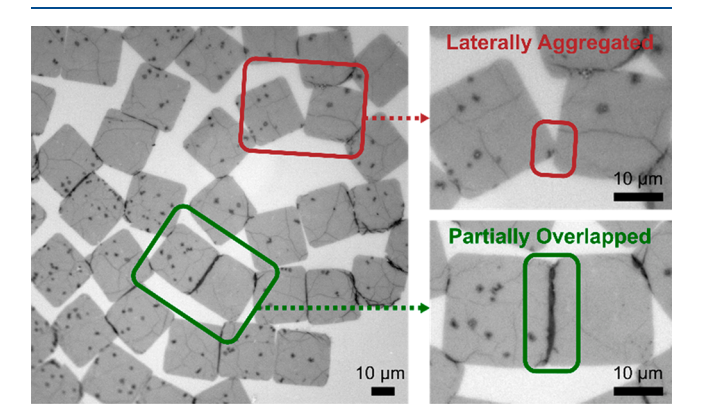


Figure 4. Experimental interference reflection microscopy image of monolayer graphene particles (25  $\mu \rm m$  squares) assembled at an air—water interface. Red boxed region (enlarged in upper right) demonstrates a region where two particles have laterally aggregated, and the green boxed region (enlarged in lower right) demonstrates a region where two particles have partially overlapped, indicated by the darker contrast in the center of the region.

under quiescent conditions at an air—water interface using an optical microscopy technique known as interference reflection microscopy. This technique provides enhanced contrast over conventional brightfield optical microscopy and enables identification of the number of graphene layers in a given region of the interface in real time, which can be used to determine when two neighboring monolayer graphene particles have either overlapped or stacked. While we do not explicitly observe any stacking events to occur, the analysis that follows is of practical significance. The assembly in Figure 4 was observed to remain laterally aggregated without stacking over a time scale of 60 min. The red, boxed region in Figure 4 depicts a location in the assembly where two particles have laterally aggregated. The contact lengths of aggregated particles within the entire image range from ~10² to ~10⁴ nm. These

contact lengths correspond to a range of free-energy barriers preventing particle stacking of  $\sim 10^2$  to  $\sim 10^4 k_B T$  (obtained from the linear fit in Figure 3c), which correspond to time scales required for these particles to stack being  $\geq 10^{28}$  s, or >10<sup>20</sup> y, obtained from the exponential fit in Figure 2d. As expected from these results, it is not surprising that we do not observe stacking of these monolayer graphene particles after only 60 min. For reference, particles with a contact edge length of 37.1 nm could theoretically be observed to overlap and stack within a 60 min time scale. In practicality, this implies that nanoscale defects could be engineered into particle edges to create regions of favorable stacking sites that could lead to directed assembly of mono- and bilayer graphene films with firm connections between particles at stacking sites. This makes liquid-phase, in situ electron microscopy studies of our system an interesting route of future work to probe these potential stacking events with enhanced spatial resolution.<sup>42</sup>

The green, boxed region in Figure 4 demonstrates a situation in which two particles have overlapped but did not transition into the completely stacked orientation during observation. Particles had become overlapped prior to initial imaging, which could have been induced by mechanical agitation during sample preparation or nanometer-scale defects along the edges of the interacting particles that encouraged particle overlap. Incomplete stacking of the particles could manifest from out-of-plane defects on either interacting particle<sup>11</sup> or sliding friction between overlapped particles.<sup>40,4</sup> Any out-of-plane defects such as oxidized functional groups or multilayer regions (seen as the dark regions within the particles in Figure 4)<sup>21</sup> can be envisioned as physical "roadblocks" that would prevent particles from continuing toward complete overlap. Additionally, the sliding friction between parallel graphene particles is dependent upon the relative orientation of stacked graphene layers with an energy barrier of  $\sim 10^{-3}$  to  $10^{-2} k_B T$  atom<sup>-1</sup> required to rotate stacked particles out of the minimum energy state.<sup>43</sup> Thus, it is feasible the particles observed in Figure 4, with one particle containing  $\sim 10^4$  C atoms along its interacting edge, could cease lateral translation if the two interacting particles adopted the most energetically favorable stacking configuration shortly after overlap.<sup>40</sup>

Our evidence presented from MD simulations and experimental results demonstrates the delicate interplay between variables affecting the stacking of monolayer graphene particles at a planar fluid-fluid interface. It is clear both the size and shape of the interacting particles determine the thermodynamics and dynamics of particle stacking once the particles are in lateral contact, but only because contact edge length is the determining factor. An interesting consequence of this is that the shape and size of two interacting particles may be identical but nanometer-scale edge defects could promote stacking when the particles adopt a certain orientation (e.g., the case when hexagonal particles adopt an edge-to-edge vs cornerto-edge orientation). Thus, it is important to note that the rotational and translational diffusivities of graphene particles, which are expected to decrease as particle size is increased, 44 should also be considered in future work as the time scales associated with particles diffusing across an interface and aligning in a given lateral orientation are important in determining the overall time scales associated with a stacking event. Additionally, the edge chemistry of practical graphene particles must be considered as most exfoliated graphene systems are likely terminated with sp<sup>3</sup>-bonded functional groups that induce additional energy barriers preventing particles from stacking. Finally, additional work aimed at expanding these results to curved fluid—fluid interfaces would be illuminating in understanding how parameters such as particle size, shape, and radius of curvature of the interface affect particle stacking at curved interfaces to engineer functional emulsions with the desired stability.

#### CONCLUSIONS

Molecular dynamics simulations were employed to understand the dynamics and thermodynamics of the stacking of monolayer graphene particles at a water-vapor interface. The time required for particles to stack was found to increase exponentially as a function of the contact edge length between interacting particles and interfacial area deformed. These results align with the Boltzmann distribution, which describes the probability of an event occurring at a given energy state. Biased simulations were performed using the adaptive biasing force algorithm to obtain the potential of mean force landscapes of the system in question. The PMF diagrams yielded two main results: the thermodynamic analysis presented in eq 1 accurately captures the change in freeenergy of the system  $\Delta E$  as two graphene particles transition from the laterally aggregated to vertically stacked state, and the free-energy barrier  $E_{\rm B}$  preventing instantaneous particle stacking is a manifestation of the surface energy penalty associated with deforming a fluid-fluid interface by a given area. We observed an increase in the magnitude of  $\Delta E$  as the surface area of the two particles increased, and an increase in  $E_{\rm B}$  with an increase in contact edge length and interfacial area deformed. Finally, we presented experimental images of selfassembled, monolayer graphene particles at an air-water interface. The self-assembled structure was stable for >60 min and no particles were observed to stack, consistent with the empirical relation in Figure 2d. The difference in length scales associated with experimental observations versus simulations explained the discrepancies previously observed regarding stacking of graphene particles in simulations, but minimal stacking in experiments. This work provides the fundamental basis for understanding a unique dynamic of 2D materials at fluid-fluid interfaces, stacking. In particular, the nanoscale edge characteristics of interacting particles are critical in preventing or encouraging stacking behavior. Thus, one could envision a route toward directed assembly of 2D particles with known contact and overlap points by patterning nanoscale features into the edges of each particle using electron beam lithography<sup>45</sup> and subsequently placing these particles at a fluid-fluid interface. We expect our work to have a broad impact on the practical implementation of 2D materials at fluid-fluid interfaces as the new knowledge from this work will enable the engineering of 2D material films with a desired thickness at a specific location within the film, which is of wide interest to those interested in creating functional 2D materialbased thin-films, emulsions, and foams.

# ASSOCIATED CONTENT

# **5** Supporting Information

The following files are available free of charge. Parameters of particles and other simulation details, independence of time to stack on particle shape, calculation of particle surface area, PMF plots with error bars, individual PMF plots of  $E_{\rm B}$  for each ABF simulation, derivation, and discussion surrounding eq 1, an empirical interaction potential for estimating the edge-to-edge interaction between graphene particles at an air—water

interface, and captions for Supporting Videos (PDF). Supporting Video 1 (AVI) Supporting Video 2 (AVI) Supporting Video 3 (AVI) The Supporting Information is available free of charge at https://pubs.acs.org/doi/10.1021/acs.jpcc.0c11447.

Parameters of particles and other simulation details, independence of time to stack on particle shape, calculation of particle surface area, PMF plots with error bars, individual PMF plots of  $E_{\rm B}$  for each ABF simulation, derivation, and discussion surrounding eeq 1, an empirical interaction potential for estimating the edge-to-edge interaction between graphene particles at an air—water interface, and captions for videos (PDF) Large hexagonal particles allowed to freely rotate and translate at a water—vapor interface (AVI)

Large hexagonal particles fixed in the corner-to-edge configuration and not allowed to rotate nor translate at a water—vapor interface (AVI)

Rectangular particles that were constrained and not allowed to rotate nor translate at a water-vapor interface (AVI)

## AUTHOR INFORMATION

## **Corresponding Author**

Joseph R. Samaniuk — Department of Chemical and Biological Engineering, Colorado School of Mines, Golden, Colorado 80401, United States; oorcid.org/0000-0002-6077-2999; Email: samaniuk@mines.edu

#### **Authors**

David M. Goggin — Department of Chemical and Biological Engineering, Colorado School of Mines, Golden, Colorado 80401, United States; o orcid.org/0000-0001-6892-2034

Ronghua Bei — Department of Chemical and Biological Engineering, Colorado School of Mines, Golden, Colorado 80401, United States; ⊚ orcid.org/0000-0002-9342-523X

Ryther Anderson – Department of Chemical and Biological Engineering, Colorado School of Mines, Golden, Colorado 80401, United States

Diego A. Gómez-Gualdrón – Department of Chemical and Biological Engineering, Colorado School of Mines, Golden, Colorado 80401, United States

Complete contact information is available at: https://pubs.acs.org/10.1021/acs.jpcc.0c11447

## **Author Contributions**

<sup>#</sup>D.M.G. and R.B. contributed equally.

#### Notes

The authors declare no competing financial interest.

## ACKNOWLEDGMENTS

Molecular simulations were made possible by the AuN supercomputer cluster at Colorado School of Mines. This work was supported by the NSF Faculty Early Career Development (CAREER) Program Award CBET-1944725.

## REFERENCES

- (1) Bonaccorso, F.; Bartolotta, A.; Coleman, J. N.; Backes, C. 2D-Crystal-Based Functional Inks. *Adv. Mater.* **2016**, 28, 6136–6166.
- (2) Wang, Q. H.; Kalantar-Zadeh, K.; Kis, A.; Coleman, J. N.; Strano, M. S. Electronics and optoelectronics of two-dimensional transition metal dichalcogenides. *Nat. Nanotechnol.* **2012**, *7*, 699–712.

- (3) Biswas, S.; Drzal, L. T. A Novel Approach to Create a Highly Ordered Monolayer Film of Graphene Nanosheets at the Liquid-Liquid Interface. *Nano Lett.* **2009**, *9*, 167–172.
- (4) Woltornist, S. J.; Oyer, A. J.; Carrillo, J. M. Y.; Dobrynin, A. V.; Adamson, D. H. Conductive Thin Films of Pristine Graphene by Solvent Interface Trapping. *ACS Nano* **2013**, *7*, 7062–7066.
- (5) Yu, X. Y.; Prevot, M. S.; Guijarro, N.; Sivula, K. Self-Assembled 2D WSe2 Thin Films for Photoelectrochemical Hydrogen Production. *Nat. Commun.* **2015**, *6*, 1–8.
- (6) Woltornist, S. J.; Varghese, D.; Massucci, D.; Cao, Z.; Dobrynin, A. V.; Adamson, D. H. Controlled 3D Assembly of Graphene Sheets to Build Conductive, Chemically Selective and Shape-Responsive Materials. *Adv. Mater.* **2017**, *29*, 1604947.
- (7) de Leon, A.; Wei, P.; Bordera, F.; Wegierak, D.; McMillen, M.; Yan, D.; Hemmingsen, C.; Kolios, M. C.; Pentzer, E. B.; Exner, A. A. Pickering Bubbles as Dual-Modality Ultrasound and Photoacoustic Contrast Agents. ACS Appl. Mater. Interfaces 2020, 12, 22308–22317.
- (8) Ardham, V. R.; Leroy, F. Atomistic and Coarse-Grained Modeling of the Adsorption of Graphene Nanoflakes at the Oil–Water Interface. *J. Phys. Chem. B* **2018**, *122*, 2396–2407.
- (9) Garbin, V.; Crocker, J. C.; Stebe, K. J. Forced Desorption of Nanoparticles from an Oil-Water Interface. *Langmuir* **2012**, 28, 1663–1667.
- (10) Razavi, S.; Cao, K. D.; Lin, B.; Lee, K. Y. C.; Tu, R. S.; Kretzschmar, I. Collapse of Particle-Laden Interfaces under Compression: Buckling vs Particle Expulsion. *Langmuir* **2015**, *31*, 7764–7775.
- (11) Cote, L. J.; Kim, F.; Huang, J. X. Langmuir-Blodgett Assembly of Graphite Oxide Single Layers. *J. Am. Chem. Soc.* **2009**, *131*, 1043–1049.
- (12) Imperiali, L.; Liao, K. H.; Clasen, C.; Fransaer, J.; Macosko, C. W.; Vermant, J. Interfacial Rheology and Structure of Tiled Graphene Oxide Sheets. *Langmuir* **2012**, *28*, 7990–8000.
- (13) Yuet, P. K.; Blankschtein, D. Molecular Dynamics Simulation Study of Water Surfaces: Comparison of Flexible Water Models. *J. Phys. Chem. B* **2010**, *114*, 13786–13795.
- (14) Srebnik, S.; Marmur, A. Negative Pressure within a Liquid–Fluid Interface Determines Its Thickness. *Langmuir* **2020**, *36*, 7943–7947.
- (15) Aarts, D.; Schmidt, M.; Lekkerkerker, H. N. W. Direct Visual Observation of Thermal Capillary Waves. *Science* **2004**, *304*, 847–850
- (16) Lehle, H.; Oettel, M. Stability and Interactions of Nanocolloids at Fluid Interfaces: Effects of Capillary Waves and Line Tensions. *J. Phys.: Condens. Matter* **2008**, *20*, 404224.
- (17) Crisafulli, A.; Khodayari, A.; Mohammadnejad, S.; Fasano, M. Sliding Dynamics of Parallel Graphene Sheets: Effect of Geometry and Van Der Waals Interactions on Nano-Spring Behavior. *Crystals* **2018**, *8*, 14.
- (18) Blair, V. E.; Celebi, K.; Müllen, K.; Vermant, J. Electrically Conductive Thin Films Derived from Bulk Graphite and Liquid—Liquid Interface Assembly. *Adv. Mater. Interfaces* **2019**, *6*, 1801570.
- (19) Zheng, Q. B.; Ip, W. H.; Lin, X. Y.; Yousefi, N.; Yeung, K. K.; Li, Z. G.; Kim, J. K. Transparent Conductive Films Consisting of Ultra large Graphene Sheets Produced by Langmuir-Blodgett Assembly. ACS Nano 2011, 5, 6039–6051.
- (20) Bresme, F.; Oettel, M. Nanoparticles at Fluid Interfaces. J. Phys.: Condens. Matter 2007, 19, 413101.
- (21) Goggin, D. M.; Zhang, H.; Miller, E. M.; Samaniuk, J. R. Interference Provides Clarity: Direct Observation of 2D Materials at Fluid–Fluid Interfaces. *ACS Nano* **2020**, *14*, 777–790.
- (22) Darve, E.; Pohorille, A. Calculating Free Energies Using Average Force. J. Chem. Phys. 2001, 115, 9169–9183.
- (23) Darve, E.; Rodríguez-Gómez, D.; Pohorille, A. Adaptive biasing force method for scalar and vector free energy calculations. *J. Chem. Phys.* **2008**, *128*, 144120.
- (24) Comer, J.; Gumbart, J. C.; Hénin, J.; Lelièvre, T.; Pohorille, A.; Chipot, C. The Adaptive Biasing Force Method: Everything You

- Always Wanted To Know but Were Afraid To Ask. J. Phys. Chem. B **2015**, 119, 1129–1151.
- (25) Martínez, L.; Andrade, R.; Birgin, E. G.; Martínez, J. M. PACKMOL: A Package for Building Initial Configurations for Molecular Dynamics Simulations. *J. Comput. Chem.* **2009**, *30*, 2157–2164.
- (26) Plimpton, S. Fast Parallel Algorithms for Short-Range Molecular Dynamics. *J. Comput. Phys.* **1995**, *117*, 1–19.
- (27) Stuart, S. J.; Tutein, A. B.; Harrison, J. A. A Reactive Potential for Hydrocarbons with Intermolecular Interactions. *J. Chem. Phys.* **2000**, *112*, 6472–6486.
- (28) Berendsen, H. J. C.; Grigera, J. R.; Straatsma, T. P. The Missing Term in Effective Pair Potentials. *J. Phys. Chem.* **1987**, *91*, 6269–6271.
- (29) Ismail, A. E.; Grest, G. S.; Stevens, M. J. Capillary Waves at the Liquid-Vapor Interface and the Surface Tension of Water. *J. Chem. Phys.* **2006**, *125*, 014702.
- (30) Vega, C.; de Miguel, E. Surface Tension of the Most Popular Models of Water by Using the Test-Area Simulation Method. *J. Chem. Phys.* **2007**, *126*, 154707.
- (31) Chen, F.; Smith, P. E. Simulated Surface Tensions of Common Water Models. J. Chem. Phys. 2007, 126, 221101.
- (32) Werder, T.; Walther, J. H.; Jaffe, R. L.; Halicioglu, T.; Koumoutsakos, P. On the Water—Carbon Interaction for Use in Molecular Dynamics Simulations of Graphite and Carbon Nanotubes. *J. Phys. Chem. B* **2003**, *107*, 1345—1352.
- (33) Hénin, J.; Fiorin, G.; Chipot, C.; Klein, M. L. Exploring Multidimensional Free Energy Landscapes Using Time-Dependent Biases on Collective Variables. *J. Chem. Theory Comput.* **2010**, *6*, 35–47.
- (34) Blake, P.; Hill, E. W.; Neto, A. H. C.; Novoselov, K. S.; Jiang, D.; Yang, R.; Booth, T. J.; Geim, A. K. Making graphene visible. *Appl. Phys. Lett.* **2007**, *91*, 063124.
- (35) Liu, I. B.; Sharifi-Mood, N.; Stebe, K. J. Capillary Assembly of Colloids: Interactions on Planar and Curved Interfaces. *Annu. Rev. Condens. Matter Phys.* **2018**, *9*, 283–305.
- (36) Israelachvili, J. N. Thermodynamic and Statistical Aspects of Intermolecular Forces. In *Intermolecular and Surface Forces*; Elsevier: USA, 2011; pp 26–29.
- (37) van Engers, C. D.; Cousens, N. E. A.; Babenko, V.; Britton, J.; Zappone, B.; Grobert, N.; Perkin, S. Direct Measurement of the Surface Energy of Graphene. *Nano Lett.* **2017**, *17*, 3815–3821.
- (38) Gonzalez, R. I.; Valencia, F. J.; Rogan, J.; Valdivia, J. A.; Sofo, J.; Kiwi, M.; Munoz, F. Bending Energy of 2D Materials: Graphene, MoS2 and Imogolite. RSC Adv. 2018, 8, 4577–4583.
- (39) Zhao, H.; Min, K.; Aluru, N. R. Size and Chirality Dependent Elastic Properties of Graphene Nanoribbons under Uniaxial Tension. *Nano Lett.* **2009**, *9*, 3012–3015.
- (40) Sinclair, R. C.; Suter, J. L.; Coveney, P. V. Graphene—Graphene Interactions: Friction, Superlubricity, and Exfoliation. *Adv. Mater.* **2018**, *30*, 1705791.
- (41) Li, W.; Moon, S.; Wojcik, M.; Xu, K. Direct Optical Visualization of Graphene and Its Nanoscale Defects on Transparent Substrates. *Nano Lett.* **2016**, *16*, 5027–5031.
- (42) Kim, P. Y.; Gao, Y.; Chai, Y.; Ashby, P. D.; Ribbe, A. E.; Hoagland, D. A.; Russell, T. P. Assessing Pair Interaction Potentials of Nanoparticles on Liquid Interfaces. *ACS Nano* **2019**, *13*, 3075–3082.
- (43) Feng, X.; Kwon, S.; Park, J. Y.; Salmeron, M. Superlubric Sliding of Graphene Nanoflakes on Graphene. *ACS Nano* **2013**, *7*, 1718–1724.
- (44) Saffman, P. G.; Delbrück, M. Brownian Motion in Biological Membranes. *Proc. Natl. Acad. Sci. U. S. A.* 1975, 72, 3111–3113.
- (45) Sommer, B.; Sonntag, J.; Ganczarczyk, A.; Braam, D.; Prinz, G.; Lorke, A.; Geller, M. Electron-Beam Induced Nano-Etching of Suspended Graphene. *Sci. Rep.* **2015**, *5*, 7781.